

Thin-disk laser scaling limit due to thermal-lens induced misalignment instability

Karsten Schuhmann^{1,2,*}, Klaus Kirch^{1,2}, Francois Nez³,
Randolf Pohl^{4,5} and Aldo Antognini^{1,2}

¹ *Institute for Particle Physics, ETH, 8093 Zurich, Switzerland*

² *Paul Scherrer Institute, 5232 Villigen-PSI, Switzerland*

³ *Laboratoire Kastler Brossel, UPMC-Sorbonne Universites, CNRS, ENS-PSL Research University, College de France, 4 place Jussieu, case 74 75005 Paris, France*

⁴ *Max Planck Institute of Quantum Optics, 85748 Garching, Germany*

⁵ *Johannes Gutenberg Universität Mainz, QUANTUM, Institut für Physik & Exzellenzcluster PRISMA, 55099 Mainz, Germany*

[*skarsten@phys.ethz.ch](mailto:skarsten@phys.ethz.ch)

Abstract: We present a fundamental obstacle in power scaling of thin-disk lasers related with self-driven growth of misalignment due to thermal lens effects. This self-driven growth arises from the changes of the optical phase difference at the disk caused by the excursion of the laser eigen-mode from the optical axis. We found a criterion based on a simplified model of this phenomenon which can be applied to design laser resonators insensitive to this effect. Moreover we propose several resonator architectures which are not affected by this effect.

1. Motivation

Thin-disk lasers (TDL) are well known for their power scalability which relates to the active medium geometry and its cooling technique [1, 2, 3]. The laser crystal is shaped as a thin disk with a diameter of typically several mm (depending on the output power/energy) and a thickness of 100 μm to 400 μm , depending on the laser active material, the doping concentration, the operation modus and the pump design. The backside of the disk is coated with dielectric layers acting as high-reflector (HR) for the laser and the pump light, and it is contacted to a water-cooled heat sink [4] as shown in Fig. 1.

As cooling occurs along the disk axis and pumping in quasi-end-pumped configuration, the heat flow in the disk points along the disk axis which is also the laser axis [1, 5]. The temperature gradients inside the laser crystal are thus mainly parallel to the laser beam axis while in radial direction the temperature within the homogeneously pumped central area is nearly uniform. Thermal lens effects are thus strongly suppressed in TDL because of the efficient cooling (large surface to volume ratio) and the small temperature gradients in radial direction. Another consequence of the disk–heat-sink geometry is that the temperature in the pumped region and therefore the thermal lens depend only on the pump power density (assuming pump diameters larger than few times the disk thickness). This is one of the fundamental properties underlying the power scalability of TDL. However, power (energy) scaling calls for an increase of the beam waist resulting in an increased sensitivity to the residual thermal lens effects which eventually limits the achievable scaling [6, 7, 8, 9, 10, 11]. When designing high power (energy)

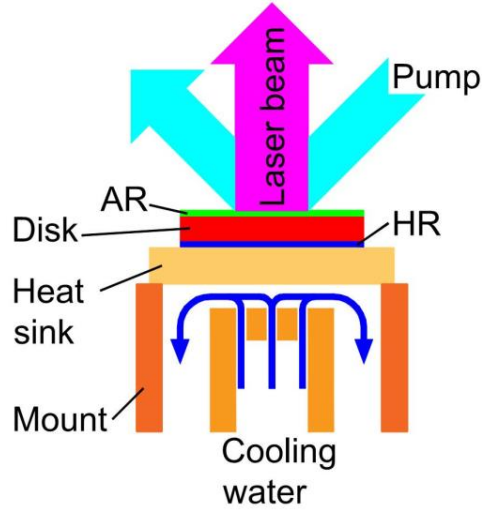


Fig. 1. (Color online) Scheme of the disk–heat-sink assembly (not to scale). The disk is thermally coupled to a water-cooled heat-sink. Cooling and temperature gradients occur along the disk axis which corresponds to the laser axis. The back and the front sides of the disk are coated with a high reflective (HR) and an anti-reflex (AR) layer, respectively for both pump and laser wavelengths.

lasers therefore it is essential to consider the stability properties of the resonator for variations of the disk thermal lens [7, 12, 13]. These are usually represented in form of so called “stability plots” [14] where the eigen-mode size at an optical element in the resonator is plotted for variations of the disk dioptric power V .

The thermal lens effect at the disk can be described using the position-dependent optical phase difference $OPD(x, y)$ experienced by the laser beam when reflecting on the disk. The outgoing (after reflection) laser field amplitude E_{out} is given by

$$E_{out}(x, y) = E_{in}(x, y) e^{g(x, y) - i \frac{2\pi}{\lambda} OPD(x, y)} \quad (1)$$

where E_{in} is the in-going (before reflection) laser field amplitude, $g(x, y)$ the space-resolved gain and λ the laser wavelength. A mathematical rigorous representation of the OPD can be accomplished using Zernike polynomials [15]. Simplifying, here we represent the one-dimensional OPD as a Taylor series

$$OPD(x) = a + bx + cx^2 + \dots \quad (2)$$

Standard resonator designs implicitly assume an OPD of the form $OPD = cx^2$, so that the disk can be described by a lens with focal length of $f = 1/(2c)$. The linear term bx is normally ignored because it simply describes the tilt of a flat optical component which is accounted implicitly in the alignment process of the laser resonator. Similarly, the constant term a produces a global phase shift which corresponds to a change of the effective length of the resonator. The dots represent higher-order contributions which have been widely discussed in the literature [8, 12, 16] as they cause beam distortion and increased losses.

In this paper we consider in more detail the interplay between the laser beam position at the active medium and the linear term bx . As detailed later, a laser beam impinging on the disk with a given deviation (excursion) from the disk–pumped-area axis induces a linear term bx in the OPD, i.e., a tilt of the disk. This tilt causes a resonator response which further modifies the position of the laser eigen-mode at the disk. For certain resonator layouts a positive feedback

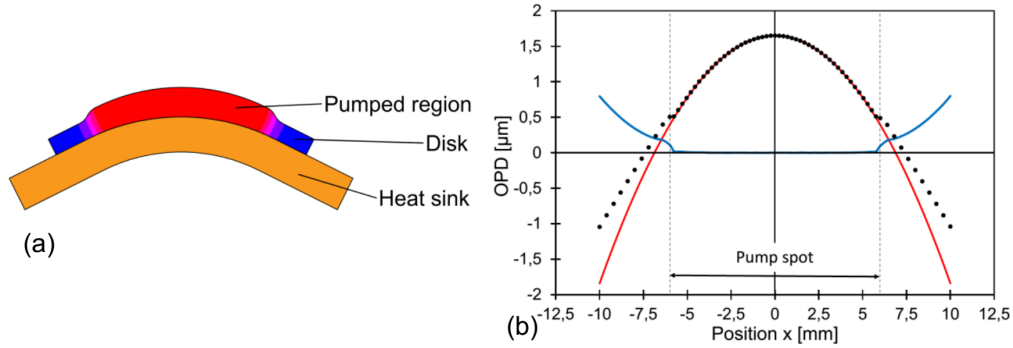


Fig. 2. (Color online) (a) Scheme (not to scale) of the bending of the disk–heat-sink assembly due to the axial temperature gradient. The “step-like” profile in laser direction is induced by the thermal expansion related to the warmer temperature within the pumped region compared with the unpumped region. (b) The dots represent the optical phase difference (OPD) at the disk computed with FEM methods for the parameters as detailed in Appendix. Only the OPD caused by the pump process (fluorescence operation) is included here. The red curve is a parabolic function fitted to the data in the central region $x \in [-3, 3]$ mm. The residual between the fit and the points is given by the solid blue line.

between tilt and laser beam position may exist which leads to a continuous growth of the eigenmode excursion at the disk resulting in a disruption of the laser operation. For other resonator configurations this interplay only leads to a finite increase of the initial excursion implying a reduced misalignment stability. A parameter will be defined to easily identify resonator designs unstable with respect to this effect, whose importance increases with the laser power.

2. Thermal lens at the disk

The rear side of the disk being at colder temperature expands (in radial direction) less than the front side causing a bending of the disk–heat-sink assembly as shown in Fig. 2 (a). We simulated OPD using finite element methods (FEM) to account for the bending of the dielectric mirror (HR) at the backside of the disk caused by this inhomogeneous radial expansion. These simulations also account for the thermal expansion of the disk in the laser direction and the variation of the disk refractive index versus temperature dn/dT .

A typical OPD simulation which includes all these effects computed using FEM as detailed in the Appendix is given in Fig. 2 (b). Within the homogeneously pumped area the OPD can be well approximated by a parabolic profile, while at the periphery of the pumped region the OPD shows a deviation from the quadratic behavior which is responsible for the excitation of higher-order beam components.

The OPD of Fig. 2 (b) considers pump effects but neglects thermal changes related to the laser operation. Indeed laser operation reduces the heat deposition in the active material as it increases the radiative de-excitation of the upper laser levels at the expense of non-radiative processes [17, 18]. Other mechanisms as a change of the effective quantum defect between laser and fluorescence operation also contribute to this effect. The model we will display in the following sections uses the effective change of the thermal lens caused by the laser operation independently of its origin.

Figure 3 (a) shows the same FEM calculation as displayed in Fig. 2 (b) but now taking into account also the reduction of the thermal load by a factor of two [17, 18, 19] due to laser operation. In this FEM computation the laser beam (resonator eigen-mode), the disk and the pumped area have a common axis. Within the laser eigen-mode (which is smaller than the pumped area) the OPD shows a quadratic behavior. Hence, in this region the disk acts as a lens whose focal

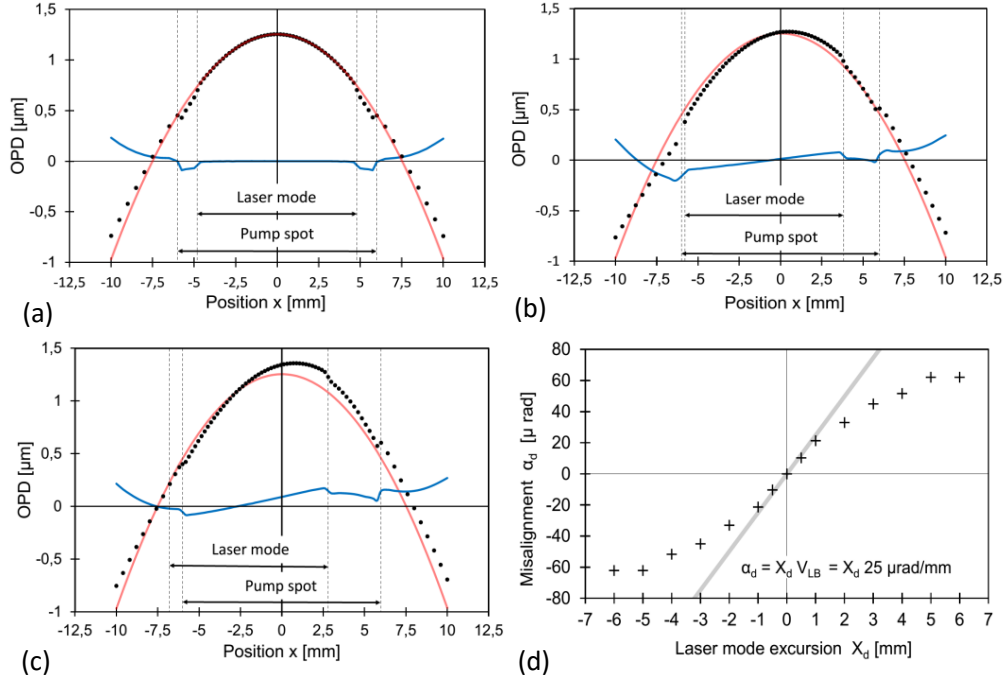


Fig. 3. (Color online) (a) The black points represent the one-dimensional optical phase difference (OPD) for a beam reflection at the disk computed with FEM methods as detailed in the Appendix. The pump and the laser beam share the same axis. The red curve is a parabolic function fitted to the FEM results in the central region $x \in [-3, 3]$ mm. This curve is used as a reference in the following panels. The difference between the fitted parabola and the simulated points is represented by the blue line. (b) Similar to (a) but in this case the laser beam impinges on the disk with an excursion of $X_d = 1$ mm from the disk–pumped-area axis. The red curve is taken from (a). (c) Similar to (b) with a beam excursion of $X_d = 2$ mm. (d) The crosses represent the angular tilt α_d of the laser beam after a reflection at the disk caused by the change of the thermal-lens due to the mode excursion X_d computed with FEM methods. The continuous line shows for comparison the prediction based on Eq. (11) with V_{LB} obtained using the same FEM calculation.

strength is smaller than in Fig. 2 (b) as expected from the decrease of heat deposition in the laser mode. The more complex structure at the periphery is related to the superposition of the effect associated with the pump and the laser mode which have been assumed to have different diameters.

The black points of Fig. 3 (b) show the OPD computed with FEM when a laser beam (laser eigen-mode) impinges on the disk 1 mm off-axis (in x -direction) relative to the disk–pumped-area axis. By subtracting from these points the quadratic function fitted to the OPD where the laser beam and the pump spot are aligned (red curve in panel (a)) a residual (blue continuous line) is obtained whose central region shows a linear behavior. This linear behavior can be interpreted as a tilt of the disk. Therefore the FEM simulation indicates that a small excursion of the laser mode from the disk–pumped-area axis induces in leading order only a tilt of the disk, while the quadratic part (focal strength) remains unchanged. This tilt grows with increasing laser eigen-mode excursion from the disk–pumped-area axis as visible by comparing Fig. 3 (b) with (c) and as summarized in (d).

In the following we use a simplified model to show that an off-axis laser beam at the active medium induces a change of the OPD that can be well approximated by a linear function with

slope different from zero. The FEM simulations have shown that the OPD caused by the pump beam alone (fluorescence operation, see Fig. 2 (b)) and by the pump beam combined with the lasing processes (see Fig. 3 (a)) in the vicinity of the disk axis can be well approximated by parabolic profiles. Thus we assume these OPDs to be of the form

$$\text{OPD}_{\text{pump}}(x) = A_{\text{pump}} + \frac{V_{\text{pump}}}{2}x^2 \quad (\text{fluorescence op.}) \quad (3)$$

$$\text{OPD}_{\text{tot}}^{\text{ONaxis}}(x) = A_{\text{tot}} + \frac{V_{\text{tot}}}{2}x^2 \quad (\text{laser operation}), \quad (4)$$

where x is the variable describing the position relative to the optical axis, V_{pump} and V_{total} are the focal strengths of the parabolic profiles, and A_{pump} , A_{tot} constants describing a global (position-independent) phase shift. The difference between these two OPDs is used to define the OPD arising from the laser beam (LB) only

$$\text{OPD}_{\text{LB}}(x) = \text{OPD}_{\text{tot}}^{\text{ONaxis}}(x) - \text{OPD}_{\text{pump}}(x) \quad (5)$$

$$= (A_{\text{tot}} - A_{\text{pump}}) + \frac{V_{\text{tot}} - V_{\text{pump}}}{2}x^2. \quad (6)$$

For TDL the thermal lens is usually defocusing because it is dominated by the bending of the disk as shown in Fig. 2 (a) so that the disk acts as a convex mirror. Consequently, for TDL the focal strength associated with the laser beam only $V_{\text{LB}} = V_{\text{tot}} - V_{\text{pump}}$ is positive (focusing)¹.

As a next step we consider the OPD resulting from the pump process and a laser beam impinging off-axis on the active medium:

$$\text{OPD}_{\text{tot}}^{\text{OFFaxis}}(x) = \text{OPD}_{\text{pump}}(x) + \text{OPD}_{\text{LB}}(x - X_d) \quad (7)$$

$$= A_{\text{tot}} + \frac{V_{\text{pump}}}{2}x^2 + \frac{V_{\text{LB}}}{2}(x - X_d)^2 \quad (8)$$

where X_d is the excursion of the laser beam from the optical axis. A misalignment of the laser beam by X_d from the disk-pumped-area axis thus gives rise to an OPD variation given by

$$\Delta(\text{OPD})(x) = \text{OPD}_{\text{tot}}^{\text{ONaxis}}(x) - \text{OPD}_{\text{tot}}^{\text{OFFaxis}}(x) \quad (9)$$

$$= +\frac{V_{\text{LB}}}{2}X_d x - \frac{V_{\text{LB}}}{2}X_d^2. \quad (10)$$

The last term in Eq. (10) is a position-independent contribution which describes an overall phase shift that can be neglected in our treatment. The first term being linear in x represents the angular tilt α_d suffered by a laser beam after reflection at the disk

$$\alpha_d = +V_{\text{LB}}X_d. \quad (11)$$

Therefore, the simplified model predicts that a beam excursion X_d at the active medium induces a tilt of $\alpha_d/2$ of the active medium proportional to the beam excursion. As well visible in Fig. 3 (d) for small excursions ($X_d \lesssim 1$ mm) there is a good agreement between the tilt calculated using only the FEM and the tilt based on Eq. (11) with V_{LB} also from the same FEM. For larger excursion this agreement decreases.

Equation (11) represents the steady state tilt of the disk caused by a fixed beam excursion. It also implies that a change of the beam excursion causes a change of the disk tilt. However, the adjustment of the disk tilt to the new beam excursion is not instantaneous but occurs with a time constant τ given by the thermalization of the disk-heat-sink assembly. For example the variation of the temperature distribution for the disk-heat-sink assembly presented in the

¹ For rod lasers the thermal lens is usually focusing because the refractive index change versus temperature is positive ($dn/dT > 0$). Hence, the reduced heat load due to laser operation leads to a negative (defocusing) V_{LB} .

Appendix has been computed to have a time constant of $\tau = 5$ ms. Due to the linearity of Eq. (11) we can model the time variation of the disk tilt as²

$$\tau \frac{d\alpha_d(t)}{dt} = V_{LB}X_d(t) - \alpha_d(t). \quad (12)$$

3. Resonator reaction for end-mirror misalignment

A geometrical ray propagating in an optical system can be described by its position $X_r(z)$ and its angle $\theta_r(z)$ with respect to the optical axis (z-axis) [20]. For an ideally aligned optical system the beam propagates along the optical axis of the system so that $X_r(z) = 0$ and $\theta_r(z) = 0$ are fulfilled everywhere. The ABCD-matrix formalism can be used to compute the beam propagation along the optical system if the initial beam position and angle are known. In a resonator the eigen-mode has to reproduce itself after a round-trip with regard to its position, angle, waist and phase front curvature.

Starting from an ideally aligned laser resonator where the laser eigen-mode is on-axis everywhere, we introduce a small misalignment of the first end-mirror by an angle $\alpha_r/2$. To have laser operation the eigen-mode position X_r and the angle θ_r at the first end-mirror must fulfill following equation

$$\begin{bmatrix} X_r \\ \theta_r \end{bmatrix} = \begin{bmatrix} D & B \\ C & A \end{bmatrix} \begin{bmatrix} A & B \\ C & D \end{bmatrix} \begin{bmatrix} X_r \\ \theta_r + \alpha_r \end{bmatrix} \quad (13)$$

where the second ABCD-matrix describes the beam propagation from the first (tilted) end-mirror to the second end-mirror, and the first ABCD-matrix the back-propagation from the second end-mirror to the first end-mirror. Note that the effective focal strength (thermal and non-thermal) of the disk is included in the two matrices. Using the condition that the determinant of each ABCD-matrix is equal to one, the solution of these equations reads

$$X_r = -\frac{\alpha_r D}{2 C} \quad (14)$$

$$\theta_r = -\alpha_r/2. \quad (15)$$

Because the resonator reaction time (10 ns time scale) is much shorter than the thermal lens adaptation time (ms time scale) we can assume that

$$X_r(t) = -\frac{\alpha_r(t) D}{2 C} \quad (16)$$

holds for any time t .

Equation (16) describes the time-dependent beam excursion at the resonator end-mirror that results as a consequence of the resonator response to a misalignment of the same end-mirror by an angle $\alpha_r/2$. This equation will be used in Sec. 4 to model the stability of a resonator having the disk as an end-mirror. For a disk used as bending mirror (for V-shaped resonators) an equation analogous to Eq. (16) has to be derived. This is accomplished in Sec. 5 and applied to resonator stability studies in Sec. 6.

²Here we implicitly assumed that there is only a single thermalization time τ , i.e., that τ does not depend on the (x, y) position because the heat flow in the active material occurs in axial (z) direction. Diamond as substrate material shows also a radial heat flow given its large thermal conductivity (see Table 3). However, this large thermal conductivity and the low thermal expansion leads to a thermal lens effects order of magnitude smaller than the one generated by the active material. Therefore, to a good approximation, only the heat flow in the laser crystal has to be considered which is along the z axis due to the moderate thermal conductivity of the active material and its small thickness. For diamond substrates the above assumption is thus justified. A metallic heat sink has a significant lower thermal conductivity compared to diamond leading to a negligible heat flow in x and y directions (assuming large pump spots). Hence, the assumption of a single thermalization time τ is fulfilled also for metallic heat sinks.

4. Resonator stability for disk as end-mirror

We have seen previously that an excursion of the eigen-mode at the disk position causes a change of the disk tilt (thermal lens effect), and that a tilt of the disk causes an excursion of the eigen-mode at the disk position (resonator reaction). Till now we neglected the interplay of these two effects. Their coupling causes a feedback loop which calls for a more detailed investigation.

Coupling of these two effects is realized by identifying

$$X \equiv X_d = X_r + X_0 \quad (17)$$

$$\alpha \equiv \alpha_d = \alpha_r. \quad (18)$$

Here we have assumed an initial eigen-mode excursion X_0 at the disk position. The magnitude of this excursion is unimportant for the understanding of the effect we are modeling in this study as will become clear later (see Eq. (21)). It must simply have a non-vanishing value: $X_0 \neq 0$. Note that this condition is always valid in practice because of the imperfection (misalignment between pump and laser mode) intrinsic in the alignment of the resonator.

By combining Eqs. (12), (16), (17) and (18) and assuming $dX_0/dt = 0$ (static or slowly varying initial misalignment) we obtain

$$\tau \frac{dX(t)}{dt} = GX(t) - [X(t) - X_0] \quad (19)$$

where we have defined the parameter G as

$$G = -\frac{V_{LB} D}{2 C}. \quad (20)$$

The solution of Eq. (19) reads:

$$X(t) = \begin{cases} X_0 \frac{G \exp\left(\frac{G-1}{\tau} t\right) - 1}{G-1} & \text{for } G \neq 1 \\ X_0 \left(1 + \frac{t}{\tau}\right) & \text{for } G=1. \end{cases} \quad (21)$$

The time behavior $X(t)$ for various values of G is plotted in Fig. 4. For $G < 0$ the initial excursion is reduced with time, for $G = 0$ it remains constant, and for $G > 0$ it is amplified. Furthermore, for $G < 1$ the initial excursion is amplified but saturates with time to a finite value, while for $G \geq 1$ the initial excursion increases continuously, $X(t \rightarrow \infty) = \infty$.

The rate of change of the excursion $\frac{dX(t)}{dt}$ depends on G , X_0 and τ . Yet the fate of the excursion at large times $X(t \rightarrow \infty)$, i.e., whether it remains constant, damped or amplified depends only on the parameter G .

We close this section by listing the various assumptions and limits underlying the analytical solution of the time evolution of the eigen-mode excursion given in Eq. (21). A linear dependence between excursion and tilt has been assumed which is valid only for small excursions ($X \lesssim 1$ mm) as demonstrated in Fig. 3 (d). We also assume a space independent time constant τ . Deviation from this behavior impact in a minor way our model as τ does not affect the fate of the beam excursion.

In this model we neglect the decrease of the circulating laser intensity caused by a misalignment. On one hand, this intensity decrease reduces V_{LB} and the tilt of the disk, on the other hand, the ratio D/C which depends on the thermal lens increases making this resonator more unstable.

In principle our model could be extended to include all these effects and the soft-aperture effects naturally occurring in the pumped medium [20, 21]. This would lead to a very complex interplay obscuring the principle of the mechanism we are disclosing in this study and whose

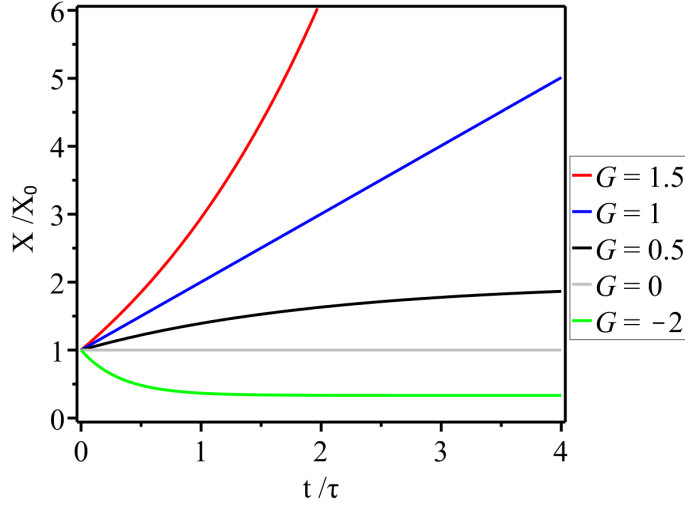


Fig. 4. (Color online) Time evolution of the eigen-mode excursion from the disk-pumped-area axis caused by the interplay between resonator reaction and change of the thermal lens due to misalignments. An initial excursion X_0 can be either reduced or amplified to a finite or infinite value depending on the value of the G parameter.

precise modeling goes beyond the scope of this paper. However, our simplified analytical model captures correctly the onset of this misalignment instability that causes a dramatic decrease of the laser performance (efficiency and stability). Thus its predictive power for designing resonator remains unaffected.

5. Stability of V-shaped resonators

In this section we investigate the stability properties of V-shaped resonators (widely used in the TDL sector [2, 12, 22, 23, 24]) with respect to the thermal-induced misalignment effect disclosed in this paper. More specifically we model here the eigen-mode excursion at the disk for a resonator where the disk is a folding mirror (not an end-mirror).

The round-trip propagation in this resonator can be divided into two branches (right and left of the disk): from the tilted disk to the second end-mirror and back to the disk

$$\begin{bmatrix} X_r' \\ \theta_r' \end{bmatrix} = \begin{bmatrix} D_R & B_R \\ C_R & A_R \end{bmatrix} \begin{bmatrix} A_R & B_R \\ C_R & D_R \end{bmatrix} \begin{bmatrix} X_r \\ \theta_r + \alpha_r \end{bmatrix}, \quad (22)$$

and from the tilted disk to the first end-mirror and back to the disk

$$\begin{bmatrix} X_r \\ \theta_r \end{bmatrix} = \begin{bmatrix} A_L & B_L \\ C_L & D_L \end{bmatrix} \begin{bmatrix} D_L & B_L \\ C_L & A_L \end{bmatrix} \begin{bmatrix} X_r' \\ \theta_r' + \alpha_r \end{bmatrix}. \quad (23)$$

The ABCD-matrixes describe the left (L) and the right (R) branches of the optical system similar to Eq. (13). The effective focal strength of the disk is included in the ABCD matrixes: it can be included without loss of generality either in the left or in the right branches or even divided between the two branches. X_r and $\theta_r + \alpha$ represent the excursion and the angle for the beam leaving the tilted disk towards the second (right) end-mirror. We assume the disk to be tilted by an angle $\alpha_r/2$. X_r' and θ_r' are the excursion and angle of the beam returning to the disk (prior to reflection on the disk) after reflection on the second end-mirror, i.e., after a propagation in the right branch. The beam leaving the disk toward the first (left) end-mirror after a reflection on the disk has thus an excursion and angle of X_r' and $\theta_r' + \alpha_r$, respectively. When it returns back at the disk after a propagation in the left branch it has an excursion X_r and an angle θ_r .

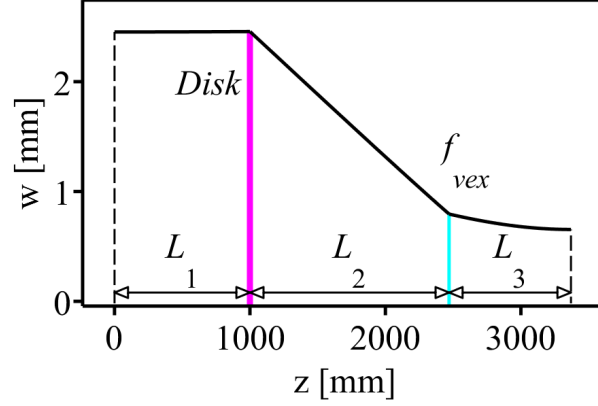


Fig. 5. (Color online) V-shaped resonator architecture consisting of a flat end-mirror, a free propagation of length L_1 , a disk with 0.5 dioptic power (in unpumped conditions), a free propagation of length L_2 , a convex lens (mirror) with focal length f_{vex} , a free propagation of length L_3 , and a flat end-mirror. The eigen-mode waist w along the resonator for a particular set of values is also given to clarify the layout.

The eigen-mode excursion at the disk position caused by a tilt of the disk by an angle $\alpha_r/2$ can be found by solving these two coupled equations and reads

$$X_r = -\alpha_r \frac{A_L D_R}{A_L C_R + C_L D_R}. \quad (24)$$

Following a similar argumentation as exposed in Sec. 4 we find that the time evolution of the excursion $X(t)$ at the disk follows Eq. (21) but with the parameter G defined as

$$G = -V_{LB} \frac{A_L D_R}{A_L C_R + C_L D_R}. \quad (25)$$

On that account, all the conclusions drawn in previous section remain valid after the appropriate replacement of the parameter G .

6. Impact on typical V-shaped resonators

One of the first steps when designing laser resonators is to study the influence of the thermal lens on the resonator stability. This is achieved usually by means of so called “stability plots” [14], i.e., by plotting the evolution of the eigen-mode size at a given optical element for variations of the thermal lens. Given a resonator layout, stable laser operation is achieved only in a limited range of thermal lens values. This range is known as the “stability region”.

In this section we illustrate the shrinkage of the effective stability region and the reduction of the output power caused by the thermal-induced misalignment mechanism. The impact of this misalignment mechanism will be illustrated for four resonator layouts, all based on the architecture sketched in Fig. 5.

For the modeling of the output power and the thermal lens effect given in Figs. 6, 7, 8, 9, 11 and 12 we have assumed the simplified situation summarized in Table 1. The thermal dioptic power of disk in laser operation has been assumed to be 50% of the thermal dioptic power in fluorescence operation [17, 18, 19] with $V_{LB} > 0$ (valid for TDL). We further assumed that the dioptic power of the disk decreases linearly with the pump power density, and that the laser operates in the fundamental mode.

Figure 6 shows the stability plot and the output power as a function of the disk dioptic power V for a resonator having an eigen-mode waist at the disk of about 1.5 mm. V accounts

Table 1. Parameters assumed to model the laser output power and the stability properties of Figs. 6, 7, 8, 9, 11 and 12. Notation: w_c is the waist of the eigen-mode in the center of the stability region, P the pump power density and V the dioptric power of the disk.

Maximal pump power density	8 kW/cm ²
Pump power density at laser threshold	0.3 kW/cm ²
Slope efficiency	50%
Pump spot diameter	$D_{\text{pump}} = 3 w_c$
Disk dioptric power (unpumped)	$V(\text{unpumped}) = 0.5 \text{ 1/m}$
Thermal dioptric power in fluorescence operation	$\frac{dV}{dP} = -0.017 \frac{1/\text{m}}{\text{kW}/\text{cm}^2}$ [19]
Thermal dioptric power in laser operation	$\frac{dV}{dP} = -0.0092 \frac{1/\text{m}}{\text{kW}/\text{cm}^2}$ [19]

Table 2. Description of significant states of the laser operation used in Figs. 6, 7, 8, 9, 11 and 12.

i	The disk is not pumped and its dioptric power is $V = 0.5 \text{ 1/m}$.
ii	The gain of the disk equals the losses at the out-coupler (other losses are neglected). Laser threshold is reached provided the resonator is within the “classical” stability region and the waist at the given dioptric power does not exceed 1.3 the layout value ($w \leq 1.3 w_c$).
iii	The disk dioptric power in <i>fluorescence</i> operation gives rise to a stable resonator with $w = 1.3 w_c$. Laser operation is starting.
iv	The disk dioptric power in <i>laser</i> operation is within the stability region with $w \approx 1.3 w_c$.
v	The parameter G becomes 1. Laser operation is disrupted giving rise to a rapid decrease of the disk dioptric power from the <i>laser</i> operation value to the <i>fluorescence</i> value (at the same pump power density).
vi	Laser operation at the maximal allowed pump power density of 8 kW/cm ² .
vi'	Laser operation at the maximal allowed pump power density of 8 kW/cm ² when the thermal induced misalignment mechanism is ignored.

for thermal and non-thermal (prior to pumping) lens effects. A qualitative understanding of the laser operation of this resonator can be obtained by considering some particular states of the laser operation indicated with Roman numbers from (i) to (vi) as summarized in Table 2.

At zero pump power (i) the dioptric power of the disk is 0.5 diopters (assumption). With increasing pump power density the dioptric power decreases. When the pump power density reaches 0.3 kW/cm² (ii) laser operation starts. A further increase the pump power density leads to an increase of the output power until the maximal allowed (due to optical damage) pump power density of 8 kW/cm² (vi) is reached. In this case, the laser resonator remains within the stability region independently of the laser pump power density. No limitations due to the above

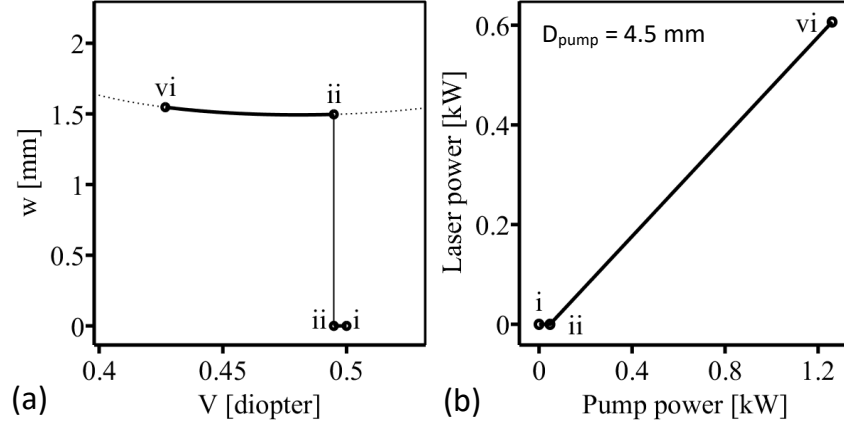


Fig. 6. (a) Eigen-mode waist at the disk versus the disk dioptric power V for a resonator layout as in Fig. 5 with $L_1 = 500$ mm, $L_2 = 1470$ mm, $L_3 = 100$ mm and $f_{\text{vex}} = -1500$ mm. The dotted line represents the “classical” stability plot, i.e., the waist w for any V . The continuous black line indicates the beam waist versus dioptric power only for the dioptric power that pertain the disk in the assumed running conditions: starting from $V = 0.5$ diopters for no pumping to $V \approx 0.42$ diopters for 8 kW/cm^2 . The value of $w = 0$ is used to indicate that at the given dioptric power there is no laser operation. The Roman numbers indicate specific states of the laser operation as described in the main text and summarized in Table 2. Between (i) and (ii) there is no laser operation because the gain at the disk in this pump power density range is still smaller than the out-coupler transmission. (b) Qualitative evolution of the output power for the resonator layout of (a) as a function of the pump power. The parameters of Table 1 have been used to model the output power evolution.

described thermal-induced misalignment are noticeable in this layout.

In Fig. 7 the output power evolution and the stability plot are given for a resonator layout whose stability region is shifted compared with the layout of Fig. 6. With increasing pump power and above the laser threshold (ii) the output power increases. However, at an output power of about 0.4 kW (v), laser operation stops because the parameter G becomes equal to 1. As a consequence, the thermal lens suddenly jumps from the laser operation value to its fluorescence value (while the pump power density remains constant). A further increase of the pump power worsen the situation because G further increases and the resonator moves out of the “classical” stability region. Also in this case, provided that the laser operation would not be disrupted by the thermal misalignment effect, the resonator would stays inside the “classical” [14] stability region for all pump power densities from 0 (i) to 8 kW/cm^2 (vi’). But for this layout the onset of the thermal-induced misalignment limits the effective stability region and the maximal output power as can be seen by comparing (v) with (vi’).

Figure 8 shows the behavior of a resonator having a larger eigen-mode waist of $w_c \approx 2.5$ mm (w_c denotes the waist in the center of the stability region). At point (ii) the disk gain becomes larger than the out-coupler losses, but there is no laser operation because the resonator lies outside of the stability region. With increasing pump power, the resonator becomes stable but laser operation starts only at point (iii) when the waist w of the eigen-mode reaches a reasonable value that we assumed to be $w = 1.3 w_c$. From (iv) to (v) the output power increases with the value given by the assumed slope efficiency and laser threshold, while from (iii) to (iv) a transition from fluorescence to efficient laser operation occurs. In this pump power density range the dioptric power of the disk can be assumed to be constant as the heat load caused by the increase of pump power density is compensated by the reduction of the heat load due to the fast growing laser output power.

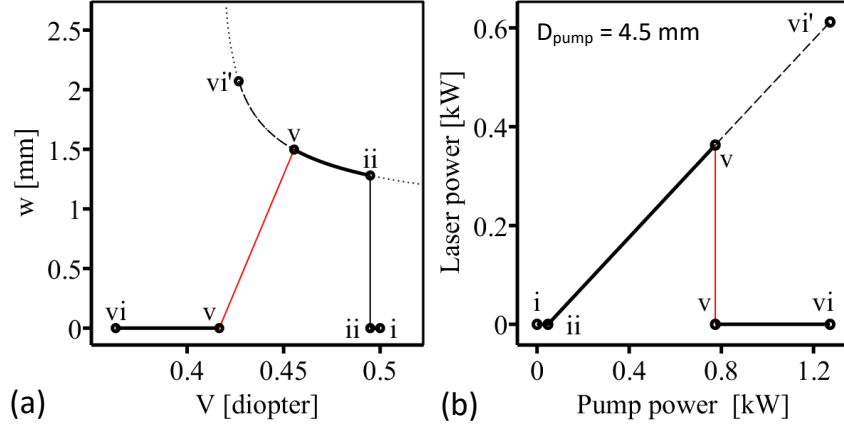


Fig. 7. (Color online) Similar to Fig. 6 but for a resonator with $L_1 = 500 \text{ mm}$, $L_2 = 900 \text{ mm}$, $L_3 = 100 \text{ mm}$ and $f_{\text{vex}} = -1500 \text{ mm}$. At position (v) the laser operation is disrupted by the onset of the thermal-induced misalignment mechanism and the dioptric power of the disk jumps from its laser operation value (0.45 diopters) to its fluorescence value (0.42 diopters) as indicated by the red line. Therefore the maximal output power reachable is limited by the onset of the misalignment mechanism presented in this study. The absence of laser operation between (i) and (ii) is because the gain at the disk does not overcome the losses at the out-coupler, while the absence of laser operation between (v) and (vi) is due to the thermal-induced misalignment. The points (vi') indicate waist and output power hypothetically reachable when neglecting the thermal-induced misalignment.

Also in this case the output power of the laser is limited by the onset of thermal-induced misalignment instabilities which occurs at position (v) when G becomes equal to 1. Here the thermal lens of the disk rapidly mutates from the laser to the fluorescence value. In this case, the obtainable maximal laser output power does not significantly deviate from the value which could be obtained at the maximal pump power density of 8 kW/cm^2 (vi'). However, for a resonator with larger eigen-mode (see Fig. 9) the limitations induced by the thermal-induced misalignment become substantial.

Laser operation of the resonator given in Fig. 9 follows the same dynamics as in Fig. 8 but shows an increased limitation arising from the thermal-induced misalignment given the shrinkage of the “classical” stability region. In fact it has been demonstrated [14] that the width of the stability region scales with $1/w_c^2$ where w_c represents the eigen-mode waist at the position of the thermal lens (disk). Hence, stable operation of high-power laser becomes increasingly challenging.

The thermal-induced misalignment effect presented here further worsens the situation because a constant (in absolute terms and independent of w) range of the stability region becomes unusable reducing the “effective” stability region. This unusable range starts from the weak focusing edge of the “classical” stability region and has a width proportional to the pump power density. This unusable range with $G \geq 1$ within the “classical” stability region is related to the commonly applied rule of thumb that a laser resonator should be designed to remain inside the stability region also when the laser cavity is blocked.

No stable laser operation is possible and power scaling reaches its limit when the width of the “classical” stability region – with increasing mode size – shrinks to the width of the unusable range (due to thermal-induced misalignment instabilities). A decrease of the pump power density would decrease the width of the unusable range allowing the use of larger eigen-mode and pump spots but the maximal output power would remain approximatively the same.

Possible non-linear variations of the thermal lens versus pump power densities [25] further

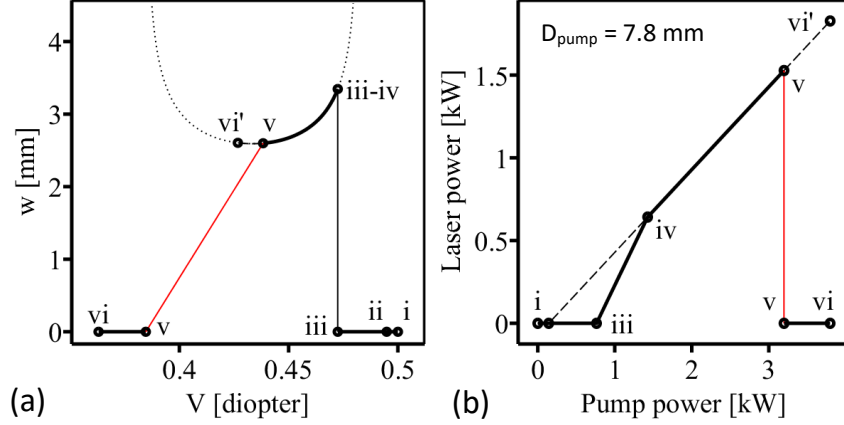


Fig. 8. (Color online) Similar to Fig. 7 but for a resonator with $L_1 = 1000 \text{ mm}$, $L_2 = 1600 \text{ mm}$, $L_3 = 900 \text{ mm}$ and $f_{\text{vex}} = -1000 \text{ mm}$. The absence of laser operation between (i) and (iii) has multiple origins: the gain at the disk does not overcome the losses at the out-coupler, or the resonator is outside the stability region, or the resonator is within the stability region but it has a waist $w > 1.3w_c$. The absence of laser operation between (v) and (vi) is due to the thermal-induced misalignment. The behavior between (iv) and (v) assumes a slope efficiency of 50% and a laser threshold of 0.3 kW/cm^2 . Between (iii) and (iv) there is a transition from fluorescence to laser operation.

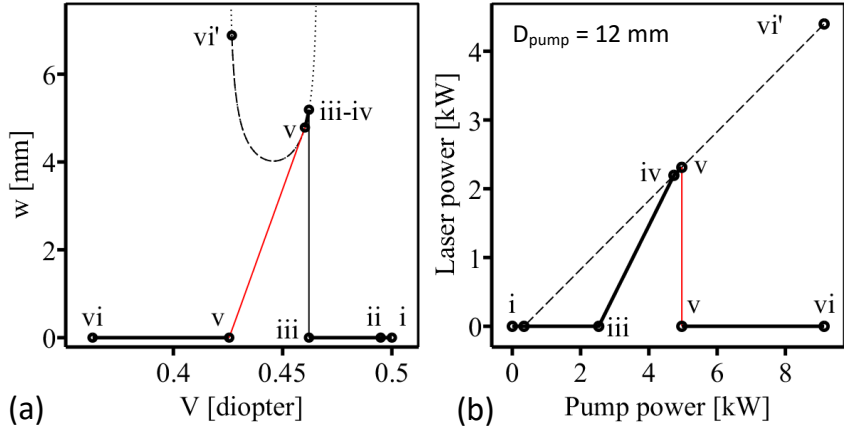


Fig. 9. (Color online) Similar to Fig. 8 but for a resonator with $L_1 = 1000 \text{ mm}$, $L_2 = 1600 \text{ mm}$, $L_3 = 2000 \text{ mm}$ and $f_{\text{vex}} = -750 \text{ mm}$.

amplifies the limiting effect of the here disclosed effect. However, proper resonator designs as exposed in the next section can be used to circumvent this problem.

7. Resonator designs insensitive to the thermal-induced misalignment

In this section we present three resonator architectures which avoid the thermal-induced misalignment by keeping $G < 1$ (assuming $V_{\text{LB}} > 0$). The resonator shown in Fig. 10 (a) has been obtained by replacing the free propagation of length L_1 on the left side of Fig. 5 by an optical segment acting as a Fourier transform. Since the ABCD-matrix of a Fourier transform based on

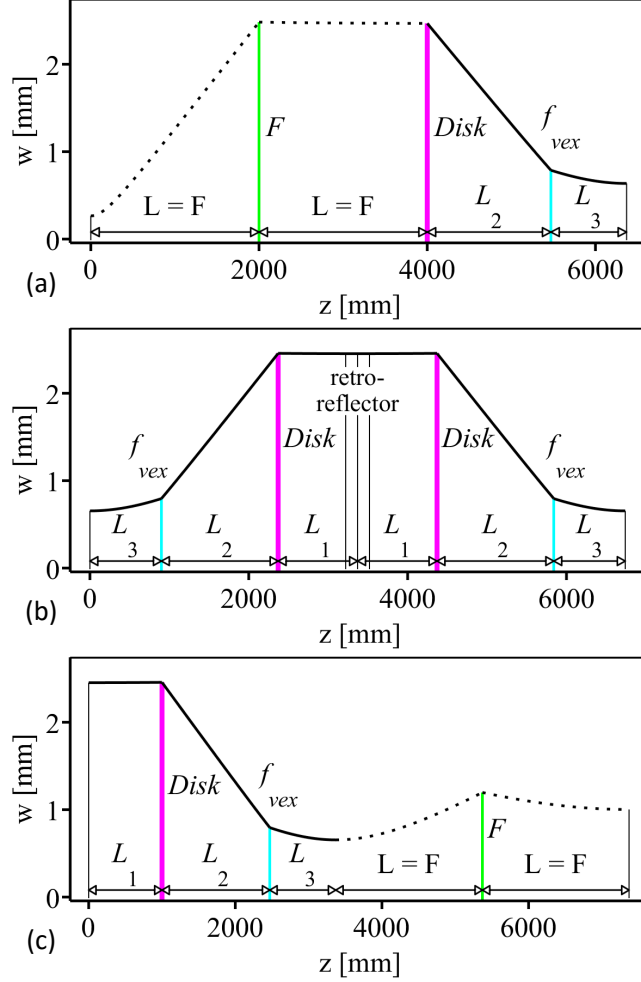


Fig. 10. (Color online) Resonator architectures with $G < 1$ (assuming $V_{LB} > 0$), i.e., unaffected by the thermal-induced misalignment. The vertical lines represent the position of the various optical elements. The eigen-mode waist w evolution along the resonator is also indicated. (a) This resonator has been obtained by replacing the left side (L_1) of the V-shaped resonator design of Fig. 5 with a Fourier-transform segment. This is achieved by inserting a focusing element with focal length F at a distance F from the disk and from the end-mirror. (b) Resonator formed by combining two identical or quasi-identical optical segments, each of which having a layout of a V-shaped resonator as in Fig. 5. A retro-reflector is placed between the two segments and the same disk has to be used in both segments [21]. (c) Similar to (a) but in this case the Fourier-transform segment is used to extend the right branch of the V-shaped resonator.

a lens of focal length F reads

$$\begin{bmatrix} A_L & B_L \\ C_L & D_L \end{bmatrix} = \begin{bmatrix} 0 & F \\ -1/F & 0 \end{bmatrix}, \quad (26)$$

the G parameter of Eq. (25) becomes zero for all layouts. The physical origin of this stabilization arises from the fact that the back and forth propagation of the beam in the Fourier segment corresponds to a $4F$ -relay imaging from pass to pass on the disk. An on-axis laser beam reflected on the disk tilted by $\alpha_r/2$ leaves the disk towards the Fourier segment with an angle

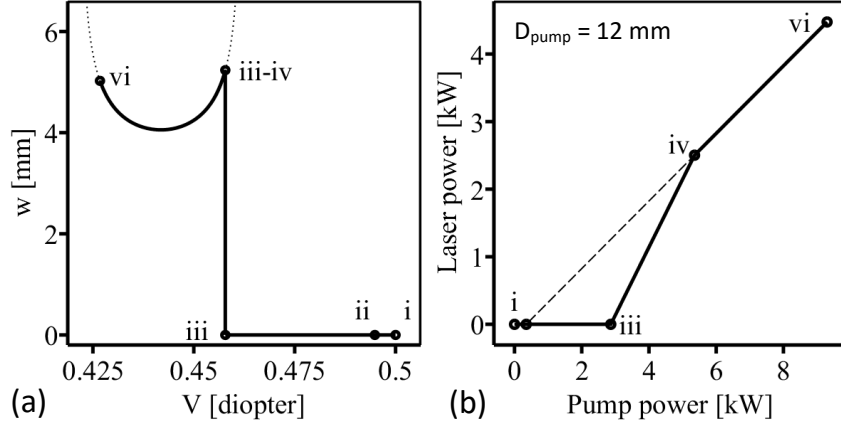


Fig. 11. Similar to Fig. 9 but with a resonator design based on Fig. 10 with $L_2 = 1620$ mm, $L_3 = 2000$ mm and $f_{\text{vex}} = -750$ mm. As for this resonator $G < 1$ (assuming $V_{\text{LB}} > 0$), the thermal-induced misalignment presented in this study does not limit the maximal output power.

$\theta_r = \alpha_r$. When the beam is coming back to the tilted disk after the propagation in the $4F$ -relay imaging system its angle is inverted so that $\theta_r = -\alpha_r$. The subsequent reflection of the beam on the disk brings the beam back on axis ($\theta_r = 0$). The beam thus reproduces itself on the right side of the resonator independently of the disk tilt.

The drawback of this architecture is that for high power resonators the cavity becomes exceedingly long. This is caused by the requirement to have large beam waist at all optical elements which calls for large F .

A retro-reflector (corner cube) as well inverts the beam angles: the beam leaving the disk with angle $\theta_r = \alpha_r$ returns after the reflection at the corner cube with an angle $\theta_r = -\alpha_r$. Therefore also the layout of Fig. 10 (b) is stable against the thermal-induced misalignment. Differently from the layout based on the Fourier extension, the propagation from disk to disk via the corner cube can be short even for large beam waists.

However, the beam offset generated by the corner cube prevents the usage of the corner cube as resonator end-mirror. For this reason in Fig. 10 (b) the corner cube is used as folding mirror between two reflections on the same disk. This resonator layout corresponds thus to a multi-pass resonator (4 reflections on the same disk per round-trip) exhibiting a larger gain compared to previous layouts. Note that the realization of this layout with two different disks would not provide any cancellation of the thermal-induced effect. Moreover it has been demonstrated that the stability region of such multi-pass resonators having only one disk does not depend on the number of reflections at the disk and have been thus proposed to solve present energy scaling of mode-locked laser oscillators [21].

In Fig. 10 (c) the Fourier-transform segment has been added to the right side of the resonator of Fig. 5. This addition leads to a sign change of G . In such a way G becomes negative stabilizing the resonator³.

The resonator adaptations presented in this section leads to larger output power and larger “effective” stability ranges as can be seen by comparing Fig. 9 with Fig. 11. This opens the way for a further increase of the waist w_c resulting in power scaling as shown in Fig. 12.

³For active media having negative V_{LB} , like rod lasers, this design leads to $G > 0$ limiting the power scaling. On the contrary the design given in Fig. 5 having $G < 0$ are power scalable for negative V_{LB} .

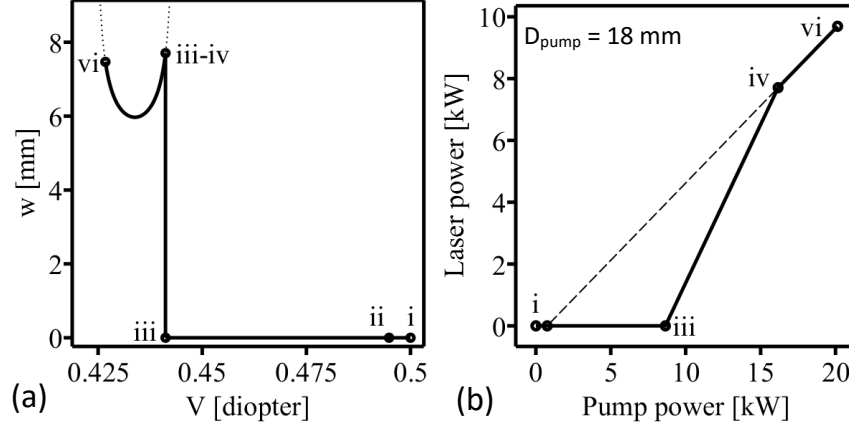


Fig. 12. Similar to Fig. 11 but with a resonator design with larger eigen-mode waist ($L_2 = 1605$ mm, $L_3 = 5000$ mm and $f_{\text{vex}} = -750$ mm).

8. Conclusion

We have exposed for the first time a fundamental obstacle to power scaling of TDL related with self-driven growth of misalignment due to thermal-lens effects. We have found a parameter G which serves to evaluate the response of an optical resonator to an excursion of the laser eigen-mode at the active medium position accounting for the changes of the OPD at the active medium caused by the excursion of the laser eigen-mode itself. This parameter G can be computed using the ABCD-matrix formalism and the knowledge of the active medium thermal lens in laser and fluorescence operation.

When designing resonator layouts the region where $G \geq 1$ has to be avoided. This results for standard TDL design (V-shaped resonator) in a restriction of the “classical” stability region (where stable laser operation can be achieved). Hence, it becomes particularly limiting for high-power TDL.

This limitation can be attenuated by reducing the thermal lens difference V_{LB} between laser operation and fluorescence operation which can be achieved by increasing the thermal conductivity of the disk–heat-sink assembly, by increasing the stiffness of the heat-sink and by lowering the heat deposition for example by using zero-phonon line pumping [25].

However, this effect can be completely avoided by suited resonator layouts as presented in Sec. 7 or by implementing an active feedback as the beam excursion grows on a time scale of milliseconds.

9. Appendix: Simulations based on finite elements methods

The thermal-induced OPD difference (at the disk) between fluorescence (only pumped) and laser operation is at the core of this study. The model we have developed describing this interplay and providing a simple criterion to characterize the sensitivity of resonators to this phenomenon assumes that a change of the eigen-mode position at the disk generates a change of its OPD which corresponds to a tilt of the disk. The FEM simulations presented in Fig. 3 demonstrate the validity of this assumption for small beam excursion ($X \lesssim 1$ mm). In this Appendix we specify the geometry and parameters entering the FEM simulations underlying the OPD profiles of Fig. 2 and Fig. 3.

To account for the asymmetry caused by the off-axis laser beam 3D simulations must be performed. This differ from typical FEM simulations [7, 6, 13] of TDL which usually assume rotational symmetry and thus are performed only along a radial cut of the disk. To reduce computing time however only half of the disk is simulated and the appropriate symmetry conditions

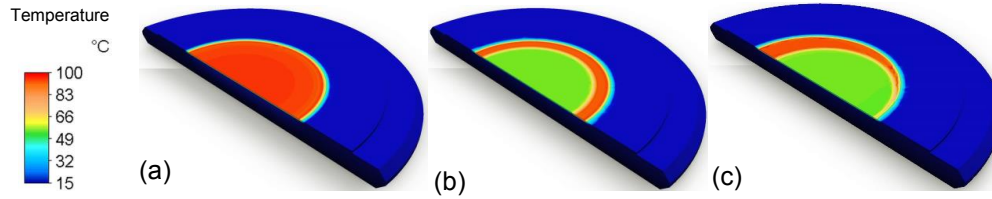


Fig. 13. (Color online) Temperature distributions of the disk–heat-sink assembly with the geometry and heat loads as specified in the main text. (a) Temperature distribution caused by the pump only. The laser is operated in fluorescence mode. (b) Laser operation reduces the heat deposited at the resonator eigen-mode position. Here the laser eigen-mode is centered relative to the pumped area while in (c) the laser eigen-mode is 1 mm off from the disk–pumped-area axis.

Table 3. Parameters assumed in the FEM simulations to model the thermal lens of the disk contacted to the diamond substrate.

Yb:YAG (7%) thermal conductivity	7 W/mK
Yb:YAG Young’s modulus	300 GPa
Yb:YAG avg. thermal expansion	8×10^{-6} 1/K
Yb:YAG refraction index change versus temperature (dn/dT)	9×10^{-6} 1/K
Diamond thermal conductivity	1900 W/mK
Diamond Young’s modulus	1100 GPa
Diamond avg. thermal expansion	9×10^{-7} 1/K

is used to extend the simulations to the whole disk. Autodesk Simulation Mechanical 2015 has been used.

The FEM simulations assume a diamond heat-sink of 1.5 mm thickness and 25 mm diameter, and an Yb:YAG active material with 140 μm thickness and a diameter of 20 mm. The heat-sink is supported at its edge, while its backside is held at a constant temperature of $T = 13$ °C. Disk coatings and contacting layers have been neglected.

A flat-top pump beam of 12 mm diameter generates a heat load of 50 W/mm³ in the active material while it is assumed that in the laser beam area (diameter of 9.6 mm) the laser beam reduces the heat load by a factor of 2. Such a reduction which strongly depends on running conditions, active medium material and pump wavelength has been observed for example in [17, 18, 19, 25, 26].

Figure 13 shows the temperature distribution at the disk surface for three different conditions computed with FEM using the parameters summarized in Table 3. In (a) the laser is in fluorescence mode, i.e., the active medium is pumped but there is no laser light produced. In transverse direction the temperature is constant within the pumped area. The heat-sink temperature is much smaller compared to the disk due to the superior conductivity of the diamond relative to Yb:YAG. In (b) the laser is operating in optimal conditions. The laser eigen-mode is perfectly aligned with the disk–pumped-area axis. As the circulating laser intensity reduces the thermal load [17, 18, 19, 25, 26] the region of superposition between pumped-area and laser eigen-mode is colder. In (c) there is a 1 mm deviation between the laser eigen-mode axis and the pumped region axis which leads to an asymmetric temperature profile. It is this asymmetric

temperature distribution which causes an asymmetric mechanical deformation of the disk back-side which produces the tilt effects described above. Adding the axial expansion of the active medium and correcting for the temperature dependence of the active medium refractive index we obtain OPD profiles whose radial cuts are shown in Fig. 2 and Fig. 3.

Funding Information

We acknowledge the support from the Swiss National Science Foundation: Projects SNF 200020.159755, SNF 200021L.138175, SNF 200021.165854, and the ERC StG. #279765.

References and links

1. A. Giesen, H. Hügel, A. Voss, K. Wittig, U. Brauch, H. Opower, *Scalable concept for diode-pumped high-power solid-state lasers*, Applied Physics B **58**, 365–372 (1994).
2. U. Brauch, A. Giesen M. Karszewski, Chr. Stewen and A. Voss, *Multiwatt diode-pumped Yb:YAG thin disk laser continuously tunable between 1018 and 1053 nm*, Opt. Lett. **20**, 713–715 (1995).
3. C. Stewen, K. Contag, M. Larionov, A. Giesen, and H. Hügel, *A 1-kW CW thin disc laser*, IEEE J. Sel. Top. Quantum Electron. **6**, 650–657 (2000).
4. J. Mende, G. Spindler, E. Schmid, J. Speiser and A. Giesen, *Thin-Disk Lasers with Dynamically Stable Resonators*, in Advanced Solid-State Photonics OSA Technical Digest Series (CD) (Optical Society of America, 2009), (2009).
5. A. Giesen and J. Speiser, *Fifteen Years of Work on Thin-Disk Lasers: Results and Scaling Laws*, Selected Topics in Quantum Electronics **13**, 598–609 (2007).
6. J. Speiser, *Thin disk laser-energy scaling*, Laser Physics **19**, 274–280 (2009).
7. J. Speiser and A. Giesen, *Numerical Modeling of High Power Continuous-Wave Yb:YAG Thin Disk Lasers, Scaling to 14 kW*, Advanced Solid-State Photonics, WB9 (2007).
8. S. Piehler, B. Weichelt, A. Voss, M. Abdou Ahmed and Thomas Graf, *Power scaling of fundamental-mode thin-disk lasers using intracavity deformable mirrors*, Opt. Lett. **37**, 5033–5035 (2012).
9. J. Mende, E. Schmid, J. Speiser, G. Spindler and A. Giesen, *Thin disk laser: power scaling to the kW regime in fundamental mode operation*, Proc. SPIE 7193, Solid State Lasers XVIII: Technology and Devices, 71931V (2009).
10. H. Fattahi, H.G. Barros, M. Gorjan et al., *Third-generation femtosecond technology*, Optica **1**, 45–63 (2014).
11. C.J. Saraceno, F. Emaury, C. Schriber, A. Diebold, M. Hoffmann, M. Golling, T. Südmeyer and U. Keller, *Toward Millijoule-Level High-Power Ultrafast Thin-Disk Oscillators*, Selected Topics in Quantum Electronics **21**, 106–123 (2015).
12. A. Antognini, K. Schuhmann, F.D. Amaro et al., *Thin-Disk Yb:YAG Oscillator-Amplifier Laser, ASE, and Effective Yb:YAG Lifetime*, Journal of Quantum Electronics, IEEE **45**, 993–1005 (2009).
13. G. Zhu, X. Zhu, M. Wang, Y. Feng and C. Zhu, *Analytical model of thermal effect and optical path difference in end-pumped Yb:YAG thin disk laser*, Appl. Opt. **53**, 6756–6764 (2014).
14. V. Magni, *Resonators for solid-state lasers with large-volume fundamental mode and high alignment stability*, Appl. Opt. **25**, 107–117 (1986).
15. J. Y. Wang and D. E. Silva, *Wave-front interpretation with Zernike Polynomials*, Appl. Opt. **19**, 1510 (1980).
16. M. R. Siegrist, M. R. Green, P. D. Morgan and R. L. Watterson, *Mode structure in the unstable resonator of an optically pumped FIR laser: an investigation*, App. Opt. **19**, 3824–3829 (1980).
17. S. Chnais, F. Druon, S. Forget, F. Balembois, P. Georges, *On thermal effects in solid-state lasers: The case of ytterbium-doped materials*, Progress in Quantum Electronics, **30**, 89–153 (2006).
18. S. Chnais, F. Balembois, F. Druon, G. Lucas-Leclin and P. Georges, *Thermal Lensing in Diode-Pumped Ytterbium Lasers Part II: Evaluation of Quantum Efficiencies and Thermo-Optic Coefficients*, Journal of Quantum Electronics, IEEE **40**, 1235 (2004).
19. J. Perchermeier and U. Wittrock, *Precise measurements of the thermo-optical aberrations of an Yb:YAG thin-disk laser*, Opt. Lett. **38**, 2422–2424 (2013).
20. A. Siegman, *Lasers*, University Science Books (1986).
21. K. Schuhmann, K. Kirch, A. Antognini, *Multi-pass oscillator layout for high-energy mode-locked thin-disk lasers*, arXiv:1603.00404 (2016).
22. F. Brunner, T. Sdmeyer, E. Innerhofer, F. Morier-Genoud, R. Paschotta, V. Kisel, V. Shcherbitsky, N. Kuleshov, J. Gao, K. Contag, A. Giesen, and U. Keller, *240-fs pulses with 22-W average power from a mode-locked thin-disk Yb:KY(WO₄)₂ laser*, Opt. Lett. **27**, 1162–1164 (2002).
23. R. Paschotta, J. Aus der Au, G.J. Spühler, S. Erhard, A. Giesen, and U. Keller, *Passive mode locking of thin-disk lasers: effects of spatial hole burning*, Appl. Phys. B **72**, 267–278 (2001).
24. C. Baer, C. Krnkel, C. Saraceno, O. Heckl, M. Golling, R. Peters, K. Petermann, T. Sdmeyer, G. Huber, and U. Keller, *Femtosecond thin-disk laser with 141 W of average power*, Opt. Lett. **35**, 2302–2304 (2010).
25. M. Smrž, T. Miura, M. Chyla, S. Nagisetty, O. Novák, A. Endo and T. Mocek, *Suppression of nonlinear phonon relaxation in Yb:YAG thin disk via zero phonon line pumping*, Opt. Lett. **39**, 4919–4922 (2014).

26. R. Peters, *Ytterbium-doped sesquioxides as highly efficient laser materials*, ISBN: 978-3-8322-8504-3, Shaker Verlag (2009).
-